Experimental and Numerical Assessment of Historical Steel-Concrete Composite Bridge Decks Without Mechanical Connectors

Mauro Poliotti[1](✉), Yuguang Yang[1], and Ane de Boer[2,3]

[1] Delft University of Technology, Delft, The Netherlands
M.Poliotti@tudelft.nl
[2] Ane de Boer Consultancy, Arnhem, The Netherlands
[3] Municipality of Amsterdam, Amsterdam, The Netherlands

Abstract. In old Dutch inner cities like Amsterdam a large number of steel-concrete bridge decks built between 1880 and 1960 remain in service nowadays and currently need assessment of their bearing capacity. A significant number of these decks were designed without any mechanical connectors like shear studs in the interface between concrete and steel. Moreover, the concrete decks were designed with only shrinkage reinforcement in both directions on the top layer of concrete. No additional transverse reinforcement was placed that can ensure proper (re)distribution of loads after cracking. In order to study the bearing capacity of this deck typology, two specimens of an existing bridge were taken to the Stevin Lab of TU Delft and tested until failure. In this work, the experimental results of both tests are presented. Then, finite element models including nonlinear behaviour of the materials and the interface are presented and compared with the experimental observations. Experimental results show that the bearing capacity is achieved after yielding of the steel beams. Nevertheless, the ductility and transverse load distribution of the elements is affected by the interface behaviour and the poor detailing. The finite element simulation strategy used shows good agreement with the experiment and can be used for future assessments.

Keywords: Experimental testing · Historical bridge · Interface behaviour · NL-FEM · Steel-concrete-composite

1 Introduction

Historical urban areas of cities like Amsterdam in The Netherlands have extended waterways, canals and rivers which are crossed by numerous old bridges. These bridges are not only part of the landmark and architectural heritage, but also key elements of the city's infrastructure, ensuring mobility of citizens and goods. Many of these bridges are more than a century old and were designed according to dated standards and to carry lighter traffic loads than the current requirements. Therefore, the safety of these bridges are of concern by the asset owners, and interventions such as reassessment, monitoring, renovation or replacement are considered.

A. Ilki et al. (Eds.): *fib* Symposium 2023, LNCE 349, pp. 1684–1694, 2023.
https://doi.org/10.1007/978-3-031-32519-9_169

A particular type of bridges that has brought attention lately is the steel-concrete-composite slab deck. These bridges were designed and built between 1880 and 1960, and around 150 are still in operation in Amsterdam [1]. These bridges are multi-span bridges, and the cross-section of the deck is composed of partially encased steel beams, see Fig. 1 and Fig. 2.

Fig. 1. Picture Bridge 70 Vijzelstraat, Amsterdam. Picture adapted from Google.

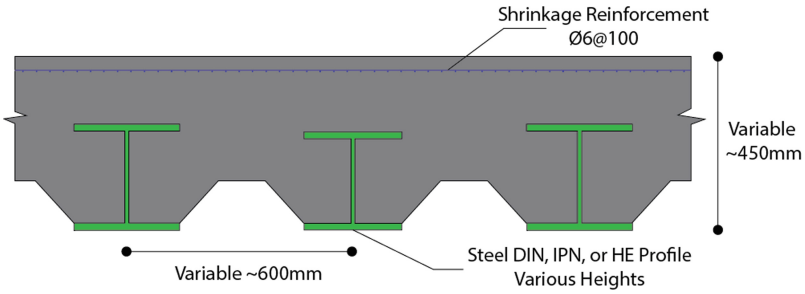

Fig. 2. Typical Cross-Section

There are two main concerns regarding the bearing capacity of these elements:

The first concern is the lack of mechanical connectors or shear studs between the steel beam and the surrounding concrete. The transfer of shear stress between steel and concrete is done only by the chemical bond and the friction of the interface. Therefore, the composite action cannot be taken into account according to current codes [2]. Nevertheless, these bridges were designed following old standards and recommendations [3, 4] where some degree of interaction is allowed even without mechanical connectors. Moreover, it has been shown [5–7] that under certain conditions it is possible to take into account the composite action.

The second challenge this concrete bridge deck typology presents is the lack of transverse reinforcement needed to ensure a proper transverse load distribution. Archive studies [1] show that small amount (usually a mesh of Ø6 every 100 mm) of reinforcement is placed on the top layer of the deck. Most likely, this was aimed to control shrinkage induced surface cracking, but it is insufficient to ensure a proper load distribution in the transverse direction. Current codes specify higher concentrated loads than the prescribed in older standards, this can produce cracking and modify the transverse distribution of

loads. This is most relevant in the outer beams of the cross section where no transverse confinement is provided by the neighbouring elements.

The lack of information on the interface behaviour as well as the lack of reinforcement makes unclear the failure mode of this type of structures. In this paper, experimental and numerical assessments are carried out to investigate the bearing capacity of this typology of bridges. First, the experimental set up is presented as well as the instrumentation. Then, the numerical simulation strategy is described. Further, results of both studies are presented and compared. Finally, conclusions on the assessment of these bridges are drawn.

2 Experimental Tests

A bridge constructed in 1934 with steel-concrete-composite deck without mechanical connectors was planned to be decommissioned as part of a renovation plan by the city of Amsterdam. Taking advantage of this, the bridge was first tested in situ [1]. The load achieved in the in situ test was limited by the foundation capacity and the global response remained on the linear range. Therefore, to investigate further the nonlinear behaviour, two additional specimens were extracted to perform testing until failure in laboratory conditions.

2.1 Specimen Description and Test Set up

The extracted specimens consist of 3 partially encased steel beams each and the total width of the specimens is approximately 2m. The shorter specimen LB1, belonged to the side span of the bridge, while the longer LB3 belonged to the main span. The two specimens differ not only on the longitudinal span but also on the cross-section height and steel beam composition. See Fig. 3 and Fig. 4.

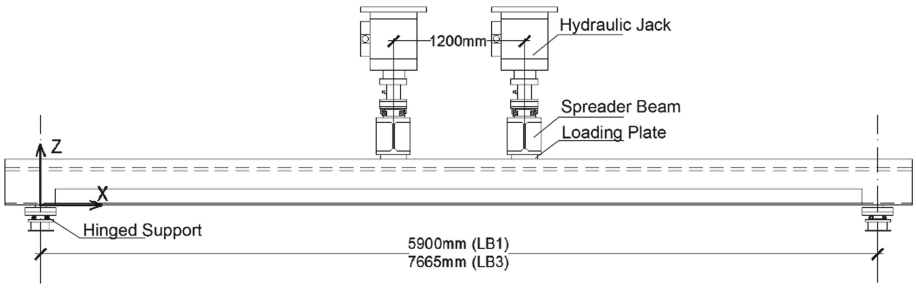

Fig. 3. Side View Specimens

Load is applied by means of two jacks following a four-point-bending scheme in longitudinal direction with a 1200 mm distance. The load of each jack is spread into two loading plates with a distance of 600 mm by a spreading beam. Therefore, load is transmitted by four loading plates of 230 × 230 mm each. Loading is applied monotonically until failure in displacement control with identical loads on both jacks. One

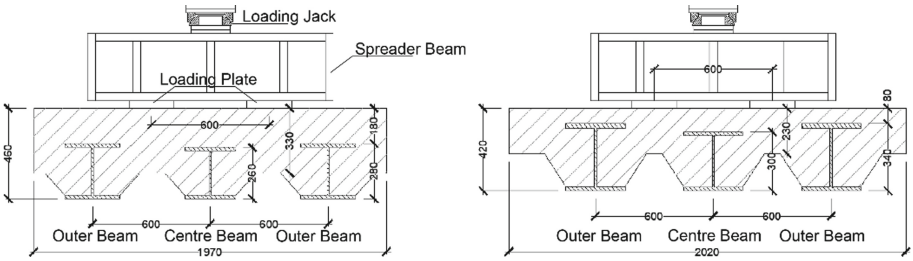

Fig. 4. Cross Sections. Left LB1. Right LB3. Dimensions in [mm]

unloading and reloading process was made on each specimen to avoid adjust the range of the sensoring system. The specimen's supports are built to ensure simply supported conditions in the longitudinal direction.

2.2 Instrumentation

The sensor plan is designed to track several key parameters of the behaviour during testing. Reactions are monitored by 6 load cells placed under the steel beams. Vertical displacements are tracked by a grid of 12 laser sensors placed under the specimen. Strains on concrete deck and steel beams are measured by means of 42 discrete optical fiber sensors with a base length of 200 mm. Steel strains are measured on the bottom flange at the center line of each beam. Concrete strains are measured on the top layer aligned vertically with the steel measurements. The interface behaviour is monitored using 8 LVDTs at different locations. At the end of beams 4 LVDTs are placed to measure the total slip between concrete and steel. Moreover, relative longitudinal slip between the

Fig. 5. Test and instrumentation. Top Left: side overview; Top Right: top view and optic fibers. Bottom Left: Bottom view transverse LVDTs; Bottom Right: Side view end LVDTs.

bottom flange and the surrounding concrete are tracked at four different locations by means of 4 LVDTs. The relative transverse displacement between the central and outer beams is measured by 6 LVDTs attached to the bottom flanges of the steel beams. Finally, 2D and 3D DIC cameras are used to monitor cracking from the side and bottom of the specimen, respectively. See Fig. 5. Full details of the measurement plan can be found in [8].

3 Numerical Simulation

Three dimensional simulations of the two specimens are made using the software DIANA FEA 10.5 [9] and following the guidelines in [10]. Taking advantage of the double symmetry of the structure, loading and support conditions, only one quarter of the structure is simulated. Horizontal displacement normal to the symmetry planes are constrained. Vertical supports are placed on the supporting steel plates. It is worth to mention that the tested specimens had a highly irregular geometry due to the removal process. Nevertheless, this is not taken into account in the model as it is not expected to have a major effect on the results.

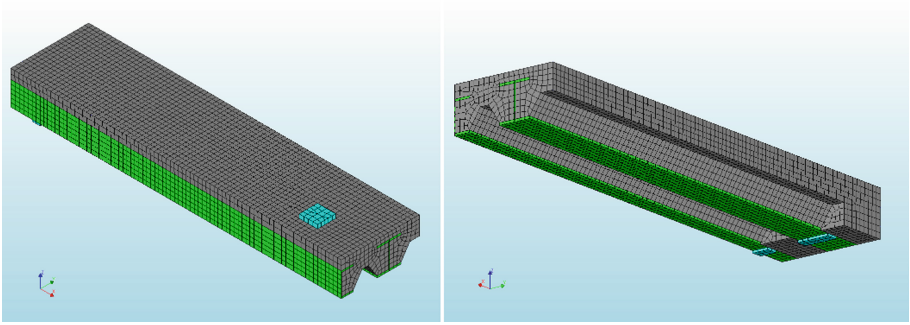

Fig. 6. Finite Element Mesh Specimen LB3, isometric views

Concrete, steel beams, and steel plates for support and loading are modeled using 20-node quadratic brick elements. 16-node quadratic interface elements are placed between the steel beams and the surrounding concrete, and on the loading and support plates. The average mesh size is set on 50 mm. See Fig. 6.

Rotating total strain crack model is used to simulate concrete behavior. Hordijk's [11] curve is used for the tensile behavior along with Govindjee's [12] definition of the crack bandwidth. Parabolic behavior with reduction due to lateral cracking is used for the compressive behavior. Parameters are estimated based on [13] and the mean compressive strength of 50.9 MPa obtained from extracted cylinders. The material behavior of the steel beams is modeled using Von-Mises plasticity with isotropic hardening. Yielding of steel is determined based on test of steel sheets extracted from the specimen. Steel plates are modeled using elastic material behavior. The mentioned material parameters are also summarized in Table 1.

Two types of interfaces are defined. The first type is the interface between plates for support and loading with the specimen. This type of interface is modeled using nonlinear elastic models with no tension and shear stiffness reduction. The second type of interface is the one between concrete and steel beams. Here, a Mohr-Coulomb friction model is used. The interface strength of concrete to steel is highly uncertain and depends on the surface treatment, shrinkage and past loading and reloading process. A cohesion value of 0.1 MPa and friction coefficient of 0.5 are used based on [13]. Nevertheless, a deeper study on these parameters is required.

A phased analysis is first made to replicate the construction process. First only the steel girders are analyzed and submitted to the self-weight of concrete. Then a second phase including the full model is analyzed introducing the test load by imposing a vertical displacement at the loading plate. A regular Newton-Raphson method is used for the nonlinear solver, with energy or out-of-balance force convergence criteria.

Table 1. Material Properties

Concrete Properties			Steel Properties		
Compressive Strength	$f_{cm} =$	50.9 MPa	Elastic Modulus	$E_s =$	200 GPa
Tensile Strength	$f_{tm} =$	3.68 MPa	Poisson Ratio	$f_{tm} =$	0.3
Elastic Modulus	$E_c =$	37 GPa	Yielding Stress	$f_y =$	235 MPa
Poisson Ratio	$\nu =$	0.2	**Interface Properties**		
Fracture Energy	$G_f =$	148 N/m	Cohesion	$c =$	0.1 MPa
Compressive Energy	$G_{fc} =$	37000 N/m	Friction	$\mu =$	0.5

4 Results and Discussion

4.1 Failure Mode Observations

During testing of both specimens yielding of the steel beams was achieved after the development of flexural cracking. Nevertheless, the observed failure mode was different for each specimen.

Specimen LB1 failed in a brittle manner after the development of plastic deformations in the steel beams. Interface failure occurred suddenly on one of the outer beams. This happened jointly with an increase of the transverse displacement between the outer and centre beams. Moreover, longitudinal cracks were observed between the beams. That also explains the increase of transverse displacements. In Fig. 7-left shows how the crack reached the end of the specimen at failure.

In the case of LB3, the specimen failed in a ductile manner exhibiting progressive concrete crushing on the top layer of concrete, see Fig. 7-rigtht.

Fig. 7. Observed Failures. Left: Specimen LB1. Right: Specimen LB3

4.2 Load Deflection

The experimental load-deflection curves of both specimens are shown and compared with the simulation results from the numerical models in Fig. 8.

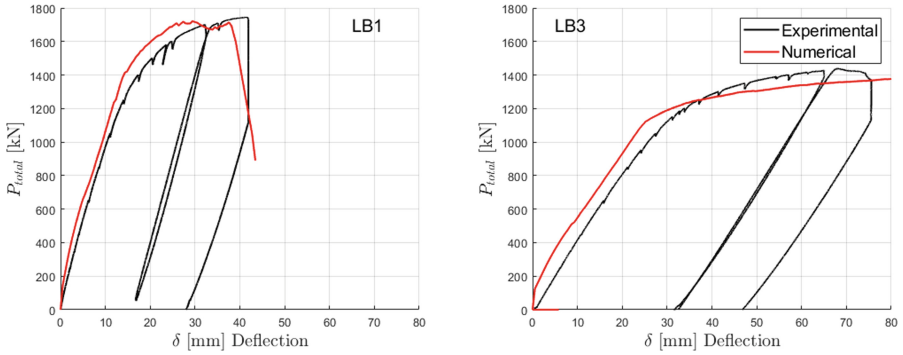

Fig. 8. Total applied load vs deflection curves obtained experimentally and numerically

Comparing both experimental curves, it can be seen that LB3 has more ductile behavior, while LB1 shows a sudden drop of its bearing capacity with limited deformation. Further, it can be seen that good agreement is obtained between numerical and experimental results in terms of maximum load and stiffness. The ductility of LB1 is also well captured by the numerical simulation.

4.3 Crack Pattern

The different failure modes relate to the different crack patterns observed. In Fig. 9-left the crack width field from numerical simulation is shown. A vertical crack on the longitudinal plane can be seen between the beams. This crack propagates until the end of the specimen and it was also experimentally observed as it can be seen in Fig. 9-right.

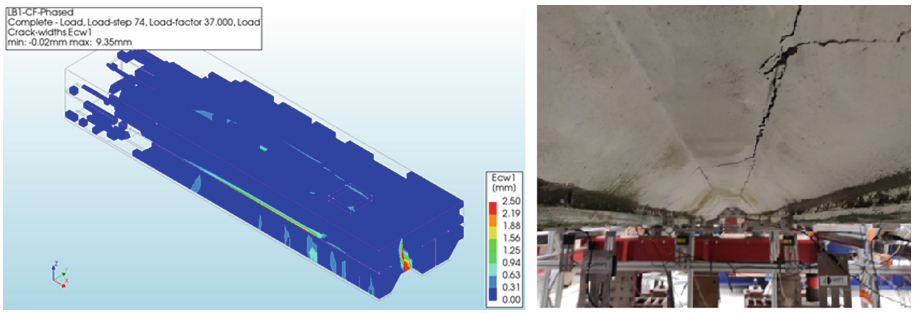

Fig. 9. Crack Pattern LB1. Left: FE isometric view. Right: Experimental bottom view

Moreover, the simulated crack width field shows an interface crack at the top flange of the center beam showing the activation of the interface.

In the case of LB3, flexural cracks are observed in the central part of the specimen in both numerical and experimental tests showing good agreement, see Fig. 10.

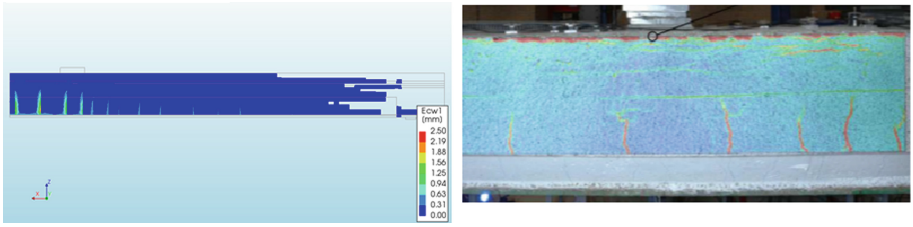

Fig. 10. Crack Pattern LB3. Left: FE side view. Right: Experimental DIC Side view

4.4 Transverse Displacement

The transverse relative displacement between bottom flanges of the central and outer beams are plotted for both specimens in Fig. 11. Comparing the experimental observations, it is shown that LB1 exhibits a much larger displacement after reaching the maximum load than LB3. This difference comes from the longitudinal crack discussed previously which is present in LB1 and not in LB3.

The outer beams are submitted to the horizontal component of the spreading of the vertical loads. In the presence of the foregoing crack, the horizontal stiffness of the outer beam decreases rapidly.

The numerical simulation agrees with the observed behaviour accurately for LB1, while it overestimates the displacement for LB3.

4.5 Interface Behaviour

Another source of difference between both specimens was the interface behaviour. In LB3 minor slips were observed during the test and on the numerical models. LB1 exhibited interface activity at early stages of the test, see Fig. 12-right.

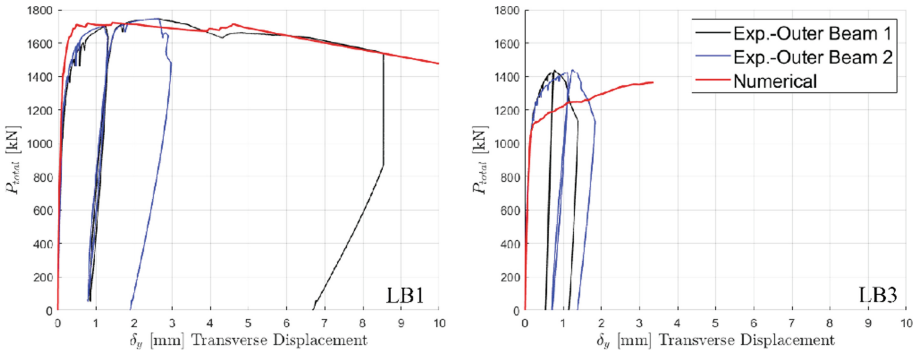

Fig. 11. Total load vs Transverse displacements between steel beams

During testing of LB1 the interface slip was distributed longitudinally but without reaching the element ends. Full propagation of the interface failure occurred at ultimate stage and on one of the outer beams, contrary to the expectation of interface failure at the more loaded centre beam.

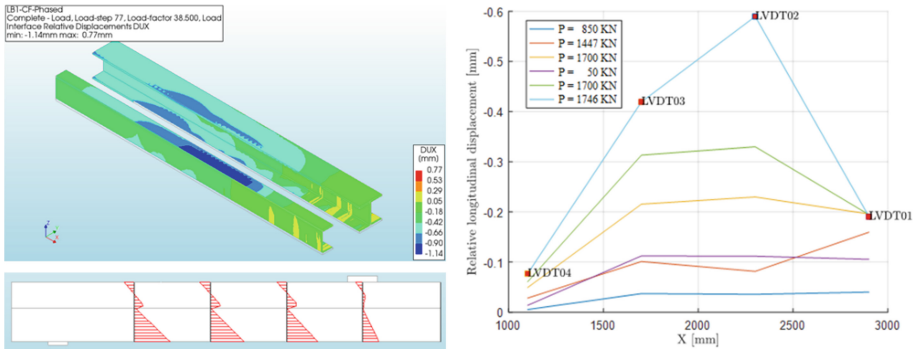

Fig. 12. Interface Behavior LB1 - Top Left: Longitudinal Interface slip. Bottom Left: Relative displacement profile at central beam. Right: Slip measurements at different locations

The overall interface behaviour was well captured by the numerical model. In Fig. 12 shows that partial interaction was simulated. A more accurate quantification of the interface behaviour requires the precise estimation of the interface parameters.

4.6 Discussion

The experiments show that in both specimens yielding of the steel beams was achieved. Nevertheless, full plastic moment was not observed on the steel beams, plastic strains reached only 80% of the web height. The occurrence of different failure modes is linked to different cross-section and material properties. The major difference that leads to different failures at ultimate stage raise from the formation and propagation of a crack between the steel beams. The interface failure occurred only after the formation of

such crack and on the outer beam rather than in the more loaded central beam. This is a consequence of the transverse cracking as, after redistribution, the outer beam is submitted to biaxial bending and torsion leading to higher interface stresses and later to failure. This is most relevant for beams located on the edge of the deck.

Numerical assessment matched experiments despite uncertain interface parameters, but improved simulation needs precise estimation of these parameters. This may not be necessary for a global assessment as lack of transverse reinforcement dominates failure.

5 Conclusions

The detailed assessment of a historical urban bridge is presented using both experimental and numerical testing. The main conclusions that can be drawn are:

1. The maximum capacity of the deck is governed by yielding of the steel elements.
2. Concrete contributes to the bearing capacity of the structure. Even though no interface connectors are placed, partial interaction exists.
3. Maximum deformation of the elements might be limited by the interface behaviour and the lack of transverse confinement.
4. The lack of transverse reinforcement can lead to cracking particularly on outer beams of the deck where no additional transverse confinement is provided. This cracking can affect the transverse load distribution.
5. The finite element modelling following the proposed simulation strategy is able to capture the different failures in a consistent way. Therefore, it can be used for future assessments and for design of strengthening interventions in similar bridges.
6. Interface properties are highly uncertain. In the case of assessment of existing structures they need to be quantified for a more accurate modelling.

Acknowledgement. The authors express their gratitude to the programme Bridges and Quay Walls of the Engineering Office of the City of Amsterdam for support of the project “Traffic load measurements”.

References

1. de Boer A, Ha, L, Quansah A (2022) Assessment by in situ load tests of historical steel-concrete bridge decks. In: Computational modelling of concrete and concrete structures, pp 712–719. CRC Press
2. CEN 2005. Eurocode 4: Design of composite steel and concrete structures - Part 1-1 General Rules and Rules for Buildings. NEN-EN 1994-1-1:2005. Brussels, Belgium: Comité Européen de Normalisation
3. Eggerman H, Kurrer K-E (2006) Zur InternationalenVerbreitung des Systems Melan seit 1892: Konstruktion und Brückenbau, Beton- und stahlbau
4. AISC-American Institute of Steel Construction (1970) Manual of Steel Construction, Seventh Edition, N. Y
5. Utescher J (1956) Bemsssungsverfahren für Verbundträger. Springer Verlag

6. Goralski C (2006) Zusammenwirken von Beton und Stahlprofil bei kammerbetonierten Verbundträgern. Ph.D. thesis RWTH, Germany
7. Watson J, O'Neil R, Barnoff RM, Mead E (1974) Composite action without shear connectors. Eng J AISC 11:29–33
8. Jørgensen A, Poliotti M, Yang Y (2022) Experiment report on steel-concrete-composite bridge deck without mechanical connectors (Verbundträger). Internal Report TU Delft. http://resolver.tudelft.nl/uuid:bf65779d-fac9-4ced-a745-047129d2d8ec
9. DIANA FEA BV (2021) DIANA User's Manual – Release 10.5. Ed. Denise Ferreira. https://manuals.dianafea.com/d105/Diana.html
10. Hendriks MAN, Roosen MA (2019) Guidelines for Nonlinear Finite Element Analysis of Concrete Structures, Rijkswaterstaat Centre for Infrastructure, Report RTD:10161:2020 v.2.2, The Netherlands
11. Hordijk DA (1991) Local approach to fatigue of concrete. Ph.D. thesis, Delft University of Technology
12. Govindjee S, Kay GJ, Simo JC (1995) Anisotropic modelling and numerical simulation of brittle damage in concrete. Int J Num Meth Eng 38:3611–3633
13. fib (2013) Model Code for Concrete Structures 2010. Fédération internationale du béton (fib). Lausanne, Switzerland